GA–A22715

EFFECTS OF ExB VELOCITY SHEAR AND MAGNETIC SHEAR IN THE FORMATION OF CORE TRANSPORT BARRIERS IN THE DIII–D TOKAMAK

by
K.H. BURRELL, M.E. AUSTIN, C.M. GREENFIELD, L.L. LAO, B.W. RICE,
G.M. STAEBLER, and B.W. STALLARD

DECEMBER 1997

DISCLAIMER

This report was prepared as an account of work sponsored by an agency of the United States Government. Neither the United States Government nor any agency thereof, nor any of their employees, makes any warranty, express or implied, or assumes any legal liability or responsibility for the accuracy, completeness, or usefulness of any information, apparatus, produce, or process disclosed, or represents that its use would not infringe privately owned rights. Reference herein to any specific commercial product, process, or service by trade name, trademark, manufacturer, or otherwise, does not necessarily constitute or imply its endorsement, recommendation, or favoring by the United States Government or any agency thereof. The views and opinions of authors expressed herein do not necessarily state or reflect those of the United States Government or any agency thereof.

EFFECTS OF ExB VELOCITY SHEAR AND MAGNETIC SHEAR IN THE FORMATION OF CORE TRANSPORT BARRIERS IN THE DIII–D TOKAMAK

by
K.H. BURRELL, M.E. AUSTIN,† C.M. GREENFIELD, L.L. LAO, B.W. RICE,‡
G.M. STAEBLER, and B.W. STALLARD‡

†University of Texas, Austin
‡Lawrence Livermore National Laboratory

This is a preprint of a paper to be presented at the IAEA Technical Committee Meeting on H–mode Physics, September 22–24, 1997, Kloster-Seeon, Germany and to be published in *Special Issue of Plasma Physics & Controlled Fusion*.

Work supported by
the U.S. Department of Energy
under Contract Nos. DE-AC03-89ER51114, W-7405-ENG-48,
and Grant No. DE-FG03-97ER54415

GA PROJECT 3466
DECEMBER 1997

ABSTRACT

Core transport barriers can be reliably formed in DIII–D by tailoring the evolution of the current density profile. This paper reports studies of the relative role of magnetic and E×B shear in creating core transport barriers in the DIII–D tokamak and considers the detailed dynamics of the barrier formation. The core barriers seen in DIII–D negative shear discharges form in a stepwise fashion during the initial current ramp. The reasons for the stepwise formation is not known; these steps do not correlate with integer values of $q(0)$ or minimum q. The data from DIII–D is consistent with previous results that negative magnetic shear facilitates the formation of core transport barriers in the ion channel but is not necessary. However, strongly negative magnetic shear does allow formation of transport barriers in particle, electron thermal, ion thermal and angular momentum transport channels. Shots with strong negative magnetic shear have produced the steepest ion temperature and toroidal rotation profiles seen yet in DIII–D. In addition, the E×B shearing rates seen in these shots exceed the previous DIII–D record value by a factor of four.

1. INTRODUCTION

The most exciting development in fusion plasma physics in the past several years is the ability to reliably and reproducibly create core transport barriers in tokamak plasmas [1–7]. Core barriers have been seen in the ion temperature, toroidal rotation, electron density and electron temperature. These examples of confinement improvement are of considerable general physical interest; it is not often that a system self-organizes to reduce transport when an additional source of free energy is applied to it. In addition to its intrinsic physics interest, the transport decrease in these shots has significant practical consequences for fusion research. For example, the best fusion performance to date in the DIII–D [8] and JT-60U [9] tokamaks has been obtained under conditions where transport reduction in the plasma core plays an important role. In the DIII–D case, for example, the ion thermal transport is at the minimum level set by standard neoclassical theory over the whole discharge [8].

Although the key to reliable production of these barriers is manipulation of the current density profile and, consequently, the magnetic shear, the model which has evolved to understand the barrier formation includes the synergistic effects of both magnetic shear and shear in the E×B drift velocity [10–12]. The negative or low magnetic shear allows stabilization of high n MHD modes (e.g. ballooning modes). In addition, the magnetic configuration with $q > 1$ everywhere stabilizes sawtooth MHD oscillations. Lack of these instabilities plus application of additional heat and, possibly, angular momentum input allows pressure and toroidal rotation gradients to build, thus increasing the radial electric field E_r and starting the feedback discussed previously [10,13] which forms the barrier. A local transport bifurcation can occur based on E×B shear decorrelation of turbulence as discussed by Staebler and Hinton [14,15]. As pointed out by Diamond *et al.* [16], the local transport bifurcation starts first in the plasma core because magnetic shear effects, $T_i/T_e > 1$ and the Shafranov shift all give the lowest threshold (microinstability growth rate) there. The transport barrier propagates outward into the region of increased microinstability growth rate until the local E×B shearing rate can no longer overcome the instability growth rate. Because E_r can be influenced by particle, angular momentum and heat input, various of these terms can be active in various machines.

Although many of the qualitative and quantitative features of core barrier formation can be understood with this model, many questions still remain. One key question that this paper investigates is the relative roles of magnetic shear and E×B shear. A second purpose of this paper is to push beyond the previously studied transition phenomena to consider the detailed dynamics of the barrier formation and expansion.

2. PHYSICS OF E_r FORMATION AND E×B SHEARING RATE

The physics which influences E_r is conventionally discussed in terms of the radial force balance equation

$$E_r = \left(Z_j \, e n_j\right)^{-1} \ \nabla \ P_j - v_{\theta j} \ B_{\phi} + v_{\phi j} \ B_{\theta} \quad , \tag{1}$$

where Z_j is the ion charge, n_j is the ion density, e is the electronic charge, P_j is the ion pressure, $v_{\theta j}$ and $v_{\varphi j}$ are, respectively, the poloidal and toroidal rotation velocities and B_θ and B_φ are, respectively, the poloidal and toroidal magnetic fields. This equation is valid for each ion species in the plasma at every point on any given flux surface; the quantities involved are local quantities.

Applying Eq. (1) to the main ions, it is clear that processes which influence the cross field transport of heat, particles and angular momentum can alter E_r and its shear. Since E×B shear influences transport according to theory, there is the possibility for several feedback loops that can bootstrap the plasma into different confinement states. These can operate either separately or together.

In order to quantitatively determine the effects of sheared E×B flow on turbulence, the E×B shearing rate needs to be compared to the turbulence decorrelation rate or the turbulence growth rate. The general toroidal geometry version of the E×B shearing rate is [18]

$$\omega_{E\times B} = \frac{\left(RB_\theta\right)^2}{B} \frac{\partial^2 \Phi}{\partial \psi^2} = -\frac{\left(RB_\theta\right)^2}{B} \ \frac{\partial}{\partial \psi} \left(\frac{E_r}{RB_\theta}\right) \tag{2}$$

Here, B is the magnitude of the magnetic field, Φ is the electrostatic potential, R is the major radius and ψ is the poloidal flux function. This definition generalizes that in Ref. [18] to a quantity which has an algebraic sign. In the turbulence stabilization theory, $\omega_{E\times B}$ enters quadratically; accordingly, the sign is not significant [18].

3. DYNAMICS OF CORE BARRIER FORMATION

Although the theory of core barrier formation [14–17] might be interpreted to indicate that transport barriers should form and expand monotonically after input power is increased, DIII–D results show that the formation process actually takes place in a stepwise fashion during the initial current ramp phase of the discharge. This is shown in Fig. 1 where two clear steps in the core ion temperature and carbon toroidal rotation occur during the initial constant power phase. This stepwise formation process is seen to take place in essentially all DIII–D shots with low or negative magnetic shear which have been examined to date. There is no MHD activity detectable on the magnetic probes during this phase of these discharges.

Theory also predicts that there should be a power threshold for core barrier formation [16,17] (More properly, this a power density threshold). As is shown in Fig. 2, this threshold must be below 2.5 MW input power for DIII–D plasmas with neutral beam injection in the direction of the plasma current. Although the steps are a bit weaker than those in Fig. 1, this shot also shows two steps in the ion temperature and toroidal rotation during the initial current ramp phase.

There has been speculation that the steps in temperature and rotation might take place when the central safety factor $q(0)$ or the minimum safety facotor q_{min} pass through integer values. This might be caused, for example, by the presence of small magnetic islands at integer q surfaces transiently degrading confinement. As can be seen in Figs. 1 and 2, while some steps do take place near integer $q(0)$ values, others do not. Accordingly, it can be concluded that this simple hypothesis is not consistent with the data. The cause of the stepwise increase is, as yet, unknown.

A similar examination of possible correlations between the steps and the q_{min} values has also been done. In general, no obvious correlation is shown with integer values of q_{min}. However, one should note that, from shot to shot, these steps are very reproducible when plasma programming is not changed. Similar steps are seen in T_e as measured with the ECE radiometer system which

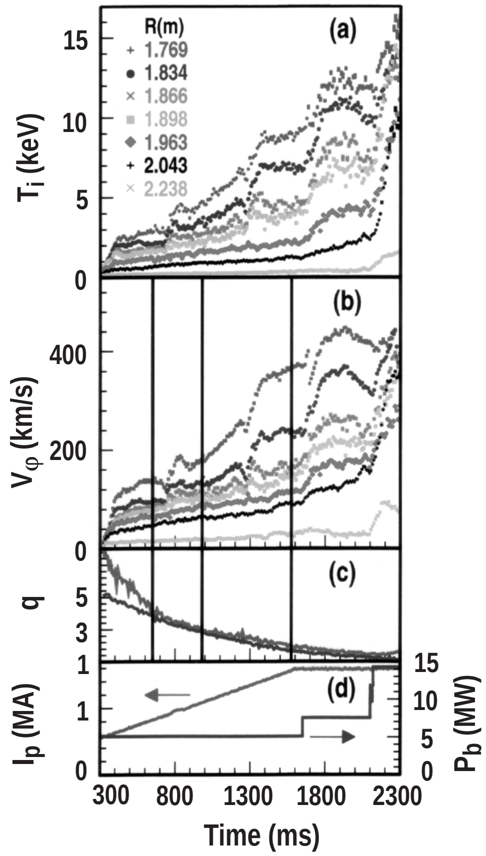

Fig. 1. Core ion temperature and carbon toroidal rotation transport barriers form in a stepwise fashion during the initial current ramp phase of shot 92528 (a) Ion temperature, (b) carbon toroidal rotation speed, (c) q-value on axis and at the minimum, (d) plasma current and neutral beam input power. Basic conditions are a toroidal field of 2.1 T and upper single null divertor with the ∇B drift away from the X–point. The plasma edge makes an L to H transition at about 2100 ms. Vertical lines in (b) and (c) indicate times when $q(0)$ passes through integer values of 2, 3 and 4.

are reproducible to within several milliseconds. Accordingly, these steps must be related to plasma variables which have similar shot to shot reproducibility.

It should be noted that all the q-values given in this paper are derived from MHD equilibrium analysis utilizing motional Stark effect (MSE) measurements to constrain the current density profile. It was discovered last year that MSE measurements could be affected by the plasma E_r [19]. All the equilibrium analysis results presented in this paper utilize the results from the upgraded MSE system where multiple spatial views are utilized to measure the E_r and correct for its effect directly in the equilibrium analysis [20].

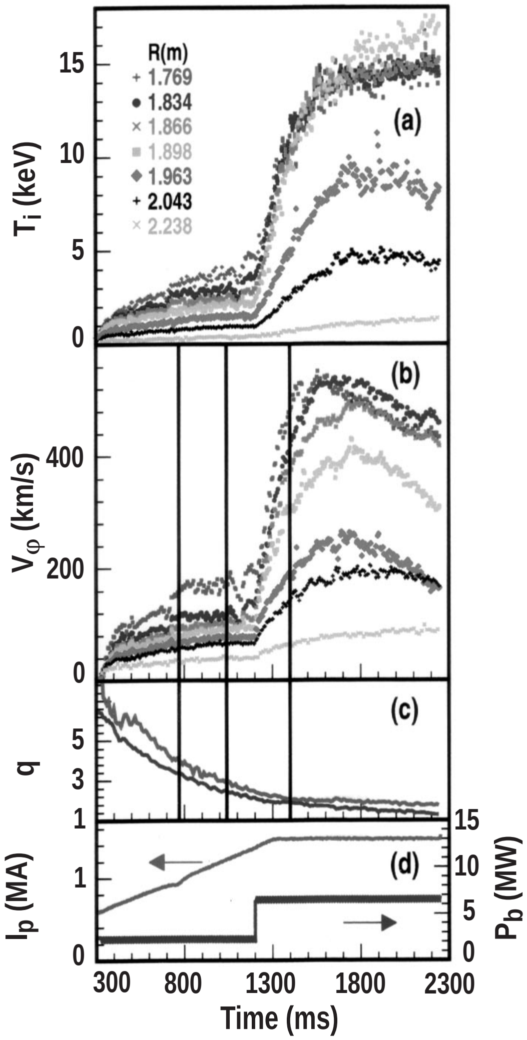

Fig. 2. Core transport barrier steps are seen even at 2.5 MW input power in shot 92691; barrier expands after power is increased. (a) Ion temperature, (b) carbon toroidal rotation speed, (c) q-value on axis and at the minimum, (d) plasma current and neutral beam input power. Basic conditions are a toroidal field of 2.1 T and upper single-null divertor with the ∇B drift away from the X–point. The plasma edge remains in L–mode throughout the time shown. Vertical lines indicate times when $q(0)$ passes through integer values of 2, 3 and 4. The small scatter of the q values indicates the magnitude of the random error due to noise on the input signals.

A key question in determining whether the steps shown in Figs. 1 and 2 occur at integer $q(0)$ or q_{min} values is the effect of errors in the q measurement. As can be seen by the width of the q traces in these two figures, the scatter in the results due to noise in the input signals is quite small. Accordingly, random errors of the magnitude indicated by the scatter would not affect this conclusion. Systematic errors are more difficult to quantify, because they depend on the fitting model chosen in the equilibrium analysis. A clearer way to confront this question is to note that, especially in Fig. 1, $q(0)$ and q_{min} pass through more integer values than there are steps in the ion temperature and rotation. While the magnitude of $q(0)$ and q_{min} at a given time is subject to possible systematic errors, the number of integer values crossed is much more accurately known. Indeed, some shots show just one transport barrier step in cases where $q(0)$ and q_{min} pass through several integer values [3].

Both Figs. 1 and 2 show that increasing the input power to the plasma causes the core barriers to expand in radius. These are consistent with previous discussions of barrier expansion and contraction with changing input power [10,21]. In Fig. 2, there is only one power increase; there are two in Fig. 1. At about the time of the the final power increase in Fig. 1, the plasma goes into H–mode and this final expansion takes place in a more dynamic plasma with an H–mode edge.

These transport barrier dynamics can shed light on another question involving the role of the shape of the q profile in core barrier formation. There are several observations in discharges with strongly reversed shear that the foot of the transport barrier appears to be locked to the point where q has a minimum (cf. [9]). This has led to speculation that the foot of the barrier is always at the minimum in q. However, the foot of the ion transport barrier is initially located well inside the radius where q is a minimum during the current ramp phase of a DIII–D shot like that in Fig. 1 [22] and only expands out to the minimum when the input power is increased. In addition, after the H–mode transition, there are cases [3,8] where ion transport is reduced to the neoclassical value across the entire plasma. In these cases, which are similar to the final phase of the shot in Fig. 1, the whole plasma exhibits reduced transport and there is, consequently, no relationship between the reduction region and particular q values. Accordingly, there are a number of counter examples to the idea that the transport barrier location is always locked to the minimum in q.

4. IS NEGATIVE MAGNETIC SHEAR NECESSARY FOR CORE TRANSPORT BARRIERS?

As is shown in Fig. 3, DIII–D data demonstrate that it is possible to create a core transport barrier in the ion transport channel even in discharges where the magnetic shear is positive and the safety factor q increases monotonically from the center to the edge of the plasma. These data are consistent with previous results from JT-60U in the high β_p mode [9]. Both the present results from DIII–D and those from JT-60U are in sawtooth-free discharges with $q(0) > 1$. Accordingly, while formation of core ion transport barriers requires enough manipulation of the current density profile to inhibit sawteeth, one does not have to produce current profiles which give negative magnetic shear.

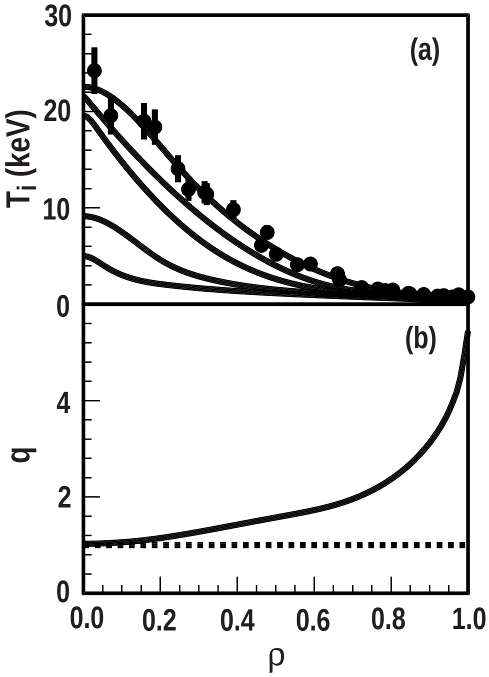

Fig. 3. Radial profiles of (a) ion temperature and (b) q for shot 89755 showing the formation and expansion of a core transport barrier in a shot with monotonic q profile. Conditions are toroidal field 2.14 T, density 1.2×10^{19} m^{-3}, plasma current 1.55 MA, beam power 10 MW in a lower single-null divertor with ∇B drift towards the X–point. The ion temperature curves are shown at times 10, 50, 100, 150, and 200 ms after the start of the 10 MW beam injection. Temperature increases monotonically with time at all positions shown. For clarity, data points are only shown on the 200 ms curve. At these times, the plasma edge is still in L–mode. The q profile is shown for the time 10 ms after the start of beam injection.

5. SHOTS WITH STRONGLY NEGATIVE MAGNETIC SHEAR

Although negative magnetic shear is not necessary for production of core ion transport barriers, several machines have reported that electron thermal transport barriers require it [6,7,9]. (In DIII–D, stronger negative magnetic shear is produced by increasing the beam power during the current ramp phase, thus raising T_e and slowing current penetration.) The DIII–D results shown in Figs. 4–6 agree with these results from other devices, although the T_e barrier shown is rather modest compared to the JT-60U result [6,9]. In addition, the results in Figs. 4 and 5 show that the steepest ion temperature gradient, carbon rotation gradient and E×B shearing rate yet measured in DIII–D occur in this shot with strongly reversed magnetic shear. The ∇T_i value, for example, is about 300 keV/m, which exceeds the H–mode edge ∇T_i by about a factor of 3. The consequence of these steep gradients is, unfortunately, increased MHD activity. Although this shot has little MHD activity at the time shown, it suffers from severe global mode activity starting about 200 ms later at a normalized β of only 1.5.

The E×B shearing rate shown in Fig. 5 is about four times bigger than the previous record value on DIII–D. One of the interesting features of this shot is how the various terms in Eq. (1) all combine to enhance the E×B shearing rate in the very core, even though some of them give positive contributions to E_r and some give negative. Notice that the final E_r given by the sum of the terms has a steeper gradient than any of the individual terms. In many cases in DIII–D, it is the toroidal rotation term that dominates E_r and, hence, the E×B shearing rate. This indicates that the feedback loop is primarily the angular momentum transport channel. However, in the present shot, it is clear that several of the feedback loops are working together to give the $\omega_{E\times B}$ seen..

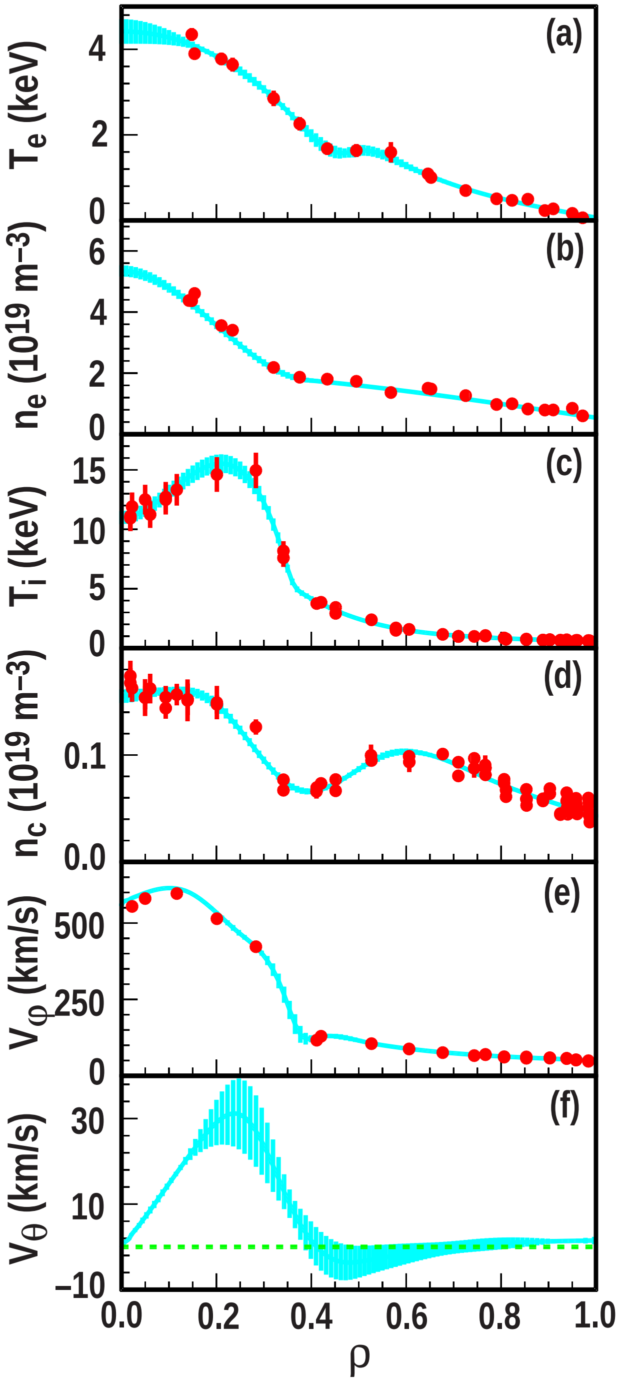

Fig. 4. Profiles of plasma parameters at 1000 ms in shot 92664 during the intial current ramp, showing transport barriers in all four transport channels. Notice the extremely steep ion temperature and carbon rotation gradients. (a) Electron temperature (b) electron density, (c) ion temperature, (d) carbon density, (e) carbon toroidal rotation, (f) carbon poloidal rotation. Basic conditions are toroidal field 2.14 T and plasma current 1.2 MA, dIp/dt = 0.9 MA/s, beam power 7.5 MW in an upper single-null divertor with ∇ B drift away from the X–point. For quantities that are not consistent on a flux surface (v_ϕ and v_θ), plots are along the outer midplane of the plasma. Vertical bars show error in input data and in spline fits.

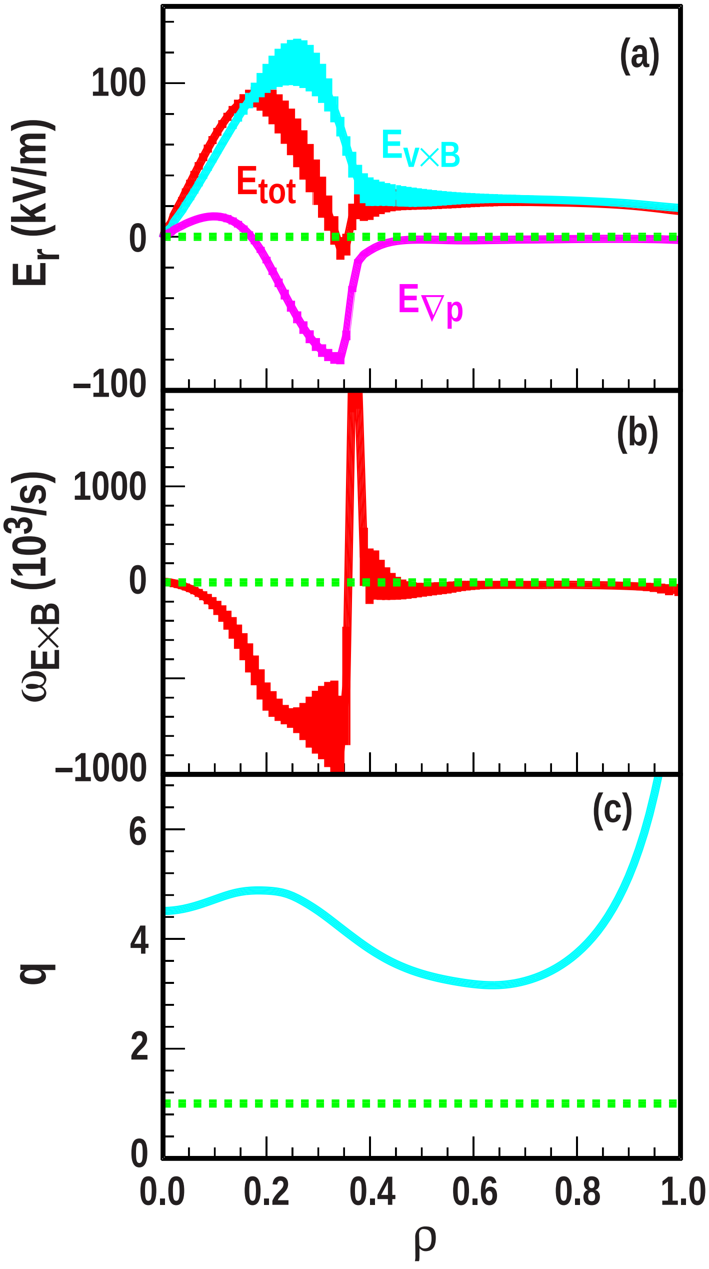

Fig. 5. Pressure gradient and toroidal rotation gradient both contribute to large E×B shear in shot 92664 at 1000 ms. (a) Total radial electric field and the pressure gradient and v x B components from Eq. (1) (b) E×B shearing rate from Eq. (2). (c) *q*-profile. Carbon density, temperature and rotation are determined from charge exchange spectroscopy while the magnetic quantities are from MHD equilibrium analysis including motional Stark effect data. Vertical bars on the curves indicate the error.

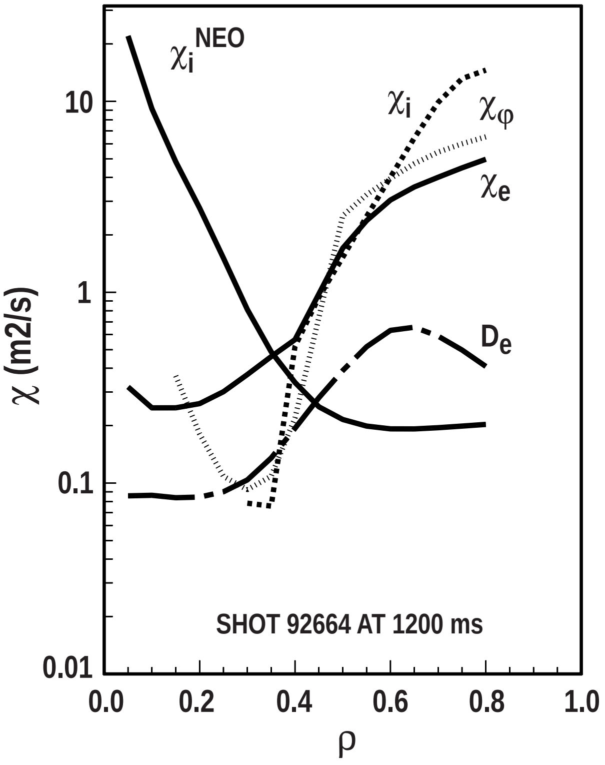

Fig. 6. Ion thermal diffusivity χ_i, electron thermal diffusivity χ_e angular momentum diffusivity χ_ϕ and electron particle diffusivity D_e determined from power balance analysis for shot 92664 at 1200 ms. This calculation was done using a time dependent transport analysis with the TRANSP code [23]. Also shown is the Chang-Hinton neoclassical predictions [24] for the ion thermal diffusivity. Note that all the difussivities show a rapid decrease near ρ=0.4 demonstrating the presence of a transport barrier in all four transport channels.

Another interesting feature of this shot is the extremely large orbit squeezing effect which is produced by the large E×B shear. Relating the theoretical squeezing parameter [25] to the E×B shearing rate in Eq. (2), we find

$$S = 1 + \frac{\omega_{E\times B}}{\omega_{ci}} \frac{B^2}{\left\langle B^2 \right\rangle} \left(\frac{B_\phi}{B_\theta} \right)^2 \qquad (3)$$

Here, ω_{ci} is the ion cyclotron frequency and $<B^2>$ denotes a flux surface average. Note that S is the same for all of the fully stripped ions usually present in a deuterium plasma, since the charge to mass ratio for all these is the same. Theory states that when $S > 0$ the banana orbit width is smaller by a factor of $S^{1/2}$ [25] and suggests that standard neoclassical ion thermal transport is reduced by a factor S. For most plasmas, S is near unity; however, in this particular case, S is about 3.4 at ρ=0.37. This may be part of the reason why such an extremely steep temperature gradient can exist.

A further important feature of this shot is the large difference that must exist between the v×B term for the deuterons and for the carbon. Equation (1) must hold for each species in the plasma. Notice that the pressure gradient term in the carbon equation has a coefficient of 1/6 while the coefficient of the analogous term in the deuteron equation is unity; these are due to the different Z_j values. Because the carbon pressure gradient contribution to E_r shown in Fig. 5 is so large even with the 1/6 coefficient, the v×B terms for the two species must differ markedly in order to result in the same E_r.

A final interesting feature of this discharge is the hollow T_i profile inside of ρ=0.3. This is a transient feature which persists for several hundred milliseconds until MHD activity sets in. The time that this feature lasts is comparable to the thermal diffusion time over this region. At present, we do not have a firm explanation for hollow profile, although, as is shown in Fig. 4, this result is well outside the measurement errors. One possibility is intense off-axis heating owing to viscous heating caused by strong toroidal velocity shear. If the deuteron velocity is significantly larger than the carbon in the steep gradient region, this could produce such heating. Unfortunately, we have no good way to accurately determine the deuteron velocity, since analysis of other shots [11] has shown that neoclassical theory does not do a good job of predicting the measured v_θ. This casts doubt on the deuteron toroidal rotation speed that, in principle, could be derived from the neoclassical equations.

As can be seen in Eq. (2), shear in the poloidal magnetic field also contributes to the overall E×B shearing rate. Because of the presence of magnetic shear in this formula, an interesting question is whether any additional effects of magnetic shear are needed to explain the improvement in electron thermal transport. It is still an open question whether additional, direct effects of magnetic shear are needed to explain the results or whether the effects of the large E×B shearing rates shown in Fig. 5 are sufficient to decorrelate the turbulence which is affecting the electron transport.

6. CONCLUSIONS

The core barriers seen in DIII–D negative shear discharges form in a stepwise fashion during the initial current ramp. The reasons for the stepwise formation is not known; these steps do not correlate with rational values of $q(0)$ or q_{min}. The data from DIII–D is consistent with previous results that negative magnetic shear facilitates the formation of core transport barriers in the ion channel but is not necessary. However, strongly negative magnetic shear does allow formation of transport barriers in particle, electron thermal, ion thermal and angular momentum transport channels. Shots with strong negative magnetic shear have produced the steepest ion temperature and toroidal rotation profiles seen yet in DIII–D. In addition, the E×B shearing rates seen in these shots exceed the previous DIII–D record value by a factor of four.

REFERENCES

[1] E.J. Strait *et al.*, 1995 Phys. Rev. Lett. **75** 4421.

[2] F.M. Levinton *et al.*, 1995 Phys. Rev. Lett. **75** 4417.

[3] L.L. Lao *et al.*, 1996 Phys. Plasmas **3**, 1951.

[4] E. Mazzucato *et al.*, 1996 Phys. Rev. Lett. **77** 3145.

[5] H. Kimura *et al.*, 1996 Phys. Plasmas **3** 1943.

[6] T. Fujita *et al.*, 1997 Phys. Rev. Lett. **78** 2377.

[7] X. Litaudon *et al.*, 1996 Plasma Phys. Contr. Fusion **38** 1603.

[8] E.A. Lazarus *et al.*, 1996 Phys. Rev. Lett. **77** 2714.

[9] Y. Koide *et al.*, 1997 Phys. Plasmas **4** 1623.

[10] K.H. Burrell, 1997 Phys. Plasmas **4** 1499.

[11] G.M. Staebler, Plasma Phys. Control. Fusion (this conference).

[12] E.J. Synakowski, Plasma Phys. Control. Fusion (this conference).

[13] K.H. Burrell, 1994 Plasma Physics and Controlled Fusion **36** A291.

[14] F.L. Hinton and G.M. Staebler, 1993 Phys. Fluids **B 5** 1281.

[15] G.M. Staebler and F.L. Hinton, 1994 Phys. Plasmas **1** 909.

[16] P.H. Diamond *et al.*, 1997 Phys. Rev. Lett **78** 1472.

[17] V. Lebedev *et al.*, 1997 in Plasma Physics and Controlled Nuclear Fusion Research 1996 (IAEA, Vienna, 1997) (to be published).

[18] T.S. Hahm and K.H. Burrell, 1995 Phys. Plasmas **2** 1648.

[19] B.W. Rice, K.H. Burrell, and L.L. Lao, 1997 Nucl. Fusion **37**, 517.

[20] B.W. Rice, K.H. Burrell, L.L. Lao, and Y.R. Lin-Liu, 1997 Phys. Rev. Lett. **79**, 2694.

[21] C.M. Greenfield *et al.*, 1997 Phys. Plasma **4** 1596.

[22] Y. Koide, K.H. Burrell, B.W. Rice, 1997 submitted to Plasma Phys. Control. Fusion.

[23] R.J. Hawryluk, in Proc. of the Course in Physics of Plasma Close to Thermonuclear Conditions, Varenna, 1979 (Commission of the European Communities, Brussels, 1980), Vol. 1, p. 19.

[24] C.S. Chang and F.L. Hinton, Phys. Fluids **29**, 3314 (1986).

[25] F.L. Hinton and Y.B. Kim, 1995 Phys. Plasmas **2** 159. cf Eq. (78).

ACKNOWLEDGMENT

Work supported by the U.S. Department of Energy under Contracts DE-AC03-89ER51114, W-7405-ENG-48 and Grant No. DE-FG03-97ER54415.